Check for updates

Importance of non-intrinsic platinum dissolution in Pt/C composite fuel cell catalysts†

Primož Jovanovič,*[ab] Urša Petek,[ac] Nejc Hodnik,[d] Francisco Ruiz-Zepeda,[a] Matija Gatalo,[ac] Martin Šala,[b] Vid Simon Šelih,[b] Tim Patrick Fellinger[e] and Miran Gaberšček (iD) *[ac]

The dissolution of different platinum-based nanoparticles deposited on a commercial high-surface area carbon (HSAC) support in thin catalyst films is investigated using a highly sensitive electrochemical flow cell (EFC) coupled to an inductively coupled plasma mass spectrometer (ICP-MS). The previously reported particle-size-dependent dissolution of Pt is confirmed on selected industrial samples with a mean Pt particle size ranging from 1 to 4.8 nm. This trend is significantly altered when a catalyst is diluted by the addition of HSAC. This indicates that the intrinsic dissolution properties are masked by local oversaturation phenomena, the so-called confinement effect. Furthermore, by replacing the standard HSAC support with a support having an order of magnitude higher specific surface area (a micro- and mesoporous nitrogen-doped high surface area carbon, HSANDC), Pt dissolution is reduced even further. This is due to the so-called non-intrinsic confinement and entrapment effects of the (large amount of) micropores and small mesopores doped with N atoms. The observed more effective Pt re-deposition is presumably induced by local Pt oversaturation and the presence of nitrogen nucleation sites. Overall, our study demonstrates the high importance and beneficial effects of porosity, loading and N doping of the carbon support on the Pt stability in the catalyst layer.

1. Introduction

The commercialization of an energy conversion based infrastructure is strongly dependent on the more general development of a hydrogen-based economy. In this sense, the performance of low-temperature proton exchange membrane fuel cells (PEMFCs) plays a very important role. This technology is already being implemented in a broad spectrum of automotive, stationary and portable applications. However, there is still a need for improvement of the performance and durability of the key components such as the membrane electrode assemblies (MEAs), membranes, catalyst layers[1] and bipolar plates.[2] During the past few decades, particular attention has been devoted to the performance of the

catalyst layer since it is estimated to constitute approximately 45% of the PEFC stack cost – due to the use of a considerable amount of expensive platinum group metals.[2] Literature data indicate that platinum nanoparticle-based electrocatalysts – while reducing effectively the required Pt amount – are not stable under harsh operating conditions at the cathode side.[3–5]

Recently, new strategies to study the catalyst layers have been developed. In large part, these strategies rely on a combinatorial approach where new analytical concepts have provided novel insights into the dissolution of platinum or more general catalyst layer degradation mechanisms.[5–12] *In situ* experimental methodologies are especially insightful, where the electrochemical treatment of the catalyst layer is coupled with one or several highly sensitive analytical tools (*e.g.* X-ray absorption spectrometers, XRD diffractometers and mass spectrometers). Recently, two groups presented a similar method called scanning flow cell or electrochemical flow cell coupled to an inductively coupled plasma mass spectrometer (SFC-ICP-MS or EFC-ICP-MS) that enable very precise (ppb) online potential- and time-resolved detection of dissolved metals.[3,8,13] Visualization of the catalyst layer has also been addressed by coupling electrochemical tools with other high resolution methods, mostly by *ex situ* approaches such as identical location transmission electron microscopy (IL-TEM)[14–18] and identical location scanning electron microscopy (IL-SEM).[19–21] There have been a few attempts to carry out *in situ* studies of

[a] Department of Materials Chemistry, National Institute of Chemistry, Hajdrihova 19, 1000 Ljubljana, Slovenia. E-mail: primoz.jovanovic@ki.si, miran.gaberscek@ki.si

[b] Department of Analytical Chemistry, National Institute of Chemistry, Hajdrihova 19, 1000 Ljubljana, Slovenia

[c] Faculty of Chemistry and Chemical Technology, University of Ljubljana, Večna pot 113, SI-1000 Ljubljana, Slovenia

[d] Department of Catalysis and Chemical reaction Engineering, National Institute of Chemistry, Hajdrihova 19, 1000 Ljubljana, Slovenia

[e] Max Planck Institute of Colloids and Interfaces, Colloids Department, Am Mühlenberg 1, Potsdam, Germany

† Electronic supplementary information (ESI) available. See DOI: 10.1039/c7cp03192k

21446 | *Phys. Chem. Chem. Phys.,* 2017, **19**, 21446–21452

This journal is © the Owner Societies 2017

electrocatalyst degradation, however this still presents a big challenge,[22] especially in a unit cell apparatus. Nevertheless, new analytical approaches have substantially improved the understanding of catalyst layer degradation. Various phenomena leading to the loss of catalyst surface area and decrease of activity, such as particle size dependent Pt dissolution, coalescence, leaching of alloying metals or carbon support corrosion, have been elucidated in great detail.[18,22–24] Based on this new knowledge, promising strategies for the mitigation of each of the known degradation mechanisms have been developed. For example, the stability of Pt nanoparticles and Pt alloys has been substantially increased by the addition of other noble metals.[25–29] Furthermore, the detrimental role of nanoparticle coalescence[5] and its circumvention by designing a microporous carbon support (exploiting the so-called confinement effect) has been reported.[30–32]

Platinum dissolution has been extensively studied before – either in the form of a polycrystalline disk[33–36] or as a nanoparticulate catalyst.[3–6,29,37–40] It has been shown that the electrochemical dissolution of Pt is predominantly a transient phenomenon occurring due to the interplay of Pt oxidation and reduction processes. These processes can be manipulated by changing the electrochemical treatment (scan rate, anodic and cathodic potential window), gas atmosphere, electrolyte, impurities, thickness of the catalyst layer,[3,33,36,37,41–44] and Pt nanoparticle size as well as by the addition of alloying metals.[3,29,37,45] Regarding the effect of Pt particle size, we have found similar results for the present samples as predicted by theory[46,47] and previously reported in the literature.[3,48,49] Specifically, under a slow potentiodynamic regime and using the same type of carbon support, dissolution was observed to be faster the smaller the Pt nanoparticles were (see ESI,† S2.1).

The effect of catalyst layer thickness on Pt dissolution, however, has only recently been proven in a conventional rotating disc electrode (RDE) study[40] by using a highly sensitive coupled analytical technique, namely SFC-ICP-MS.[39] Quite surprisingly, using these highly sensitive methods and systematically varying the catalyst loading of the electrodes showed that the Pt dissolution rate decreased as the loading increased. This was attributed to (i) an increased probability of Pt ions being trapped inside rather than diffusing out of the porous catalyst layer when the loading was higher. Consequently, the re-deposition of Pt species in a cathodic scan lowered the overall dissolution and masked the so-called intrinsic dissolution. Additionally, (ii) due to the subsequent increased concentration of Pt ions in the pores of the catalyst layer, the equilibrium dissolution potential shifted as predicted by the Nernst equation. This resulted in lower dissolution rates when a thicker catalyst layer was present.[39]

Recently, extensive investigation of Pt nanoparticles on high surface area carbon supports, such as nitrogen doped hollow graphitic spheres (Pt/HGS), has shown that particles of sizes smaller than 5 nm exhibit excellent stability under a variety of degradation conditions.[5] The increased stability in comparison to benchmark Pt/C catalysts has been ascribed to the confinement of particles inside the mesoporous matrix of HGS. Additionally, some studies indicated that the improved stability in N-doped vs. non-doped carbons was due to a better dispersion of Pt nanoparticles which inhibited agglomeration of Pt during electrochemical testing[50,51] (and references therein). Finally, some studies involving N-doped carbon supports only showed an increased initial activity but no particular improvement in catalyst stability.[31] Even though performed in a simple half-cell configuration, these studies shed new light on the extensive complexity of the catalyst composite dissolution process. This calls for further investigation before real catalyst layers should be designed.

In the present work, we are further elucidating several aspects of the Pt dissolution mechanism utilizing EFC-ICP-MS on three commercially available industrial Pt/C catalysts. Additionally, we use the same analytical tool on a novel, highly-porous nitrogen doped carbon Pt composite (Pt@HSANDC) and demonstrate the stabilizing effect of the high surface area carbon support with large amounts of micro- and small mesopores doped with N atoms on the dissolution of Pt nanoparticles.

2. Experimental

2.1 Electrochemical flow cell coupled to ICP-MS

The dissolution of Pt from the catalysts of interest was investigated using a BASi electrochemical flow cell (the Cross-Flow Cell Kit MW-5052 with a dual 3 mm glassy carbon GC electrode) coupled with an Agilent 7500ce ICP-MS instrument (Agilent Technologies, Palo Alto, USA) equipped with a MicroMist glass concentric nebulizer and a Peltier-cooled Scott-type double-pass quartz spray chamber. A forward radio frequency power of 1500 W was used with the following Ar gas flows: carrier of 0.85 L min^{-1}, makeup of 0.28 L min^{-1}, plasma of 1 L min^{-1}, and cooling of 15 L min^{-1}. The HClO$_4$ (0.1 mol L^{-1}, Aldrich 70%, 99.999% trace metals basis) carrier solution for the electrochemical experiments was pumped at 263 mL min^{-1} by using a peristaltic pump into the BASi EC flow cell and then directly into the nebulizer of the ICP-MS. The carrier solution and the electrochemical cell were electrically grounded with respect to the ICP-MS to minimize the possibility of ICP-MS response spikes from static charging at the peristaltic pump rollers. The ICP-MS was tuned for high sensitivity to obtain the best possible signal-to-noise ratio for the measurements.

The concentration of the catalyst ink was set to 1 mg mL^{-1}. The suspension was drop casted by a micropipette on one of the GC electrodes and stabilized by 5 μL of Nafion® (5 wt% water suspension) diluted with isopropanol (1/50). The second GC electrode was used as a counter electrode. The orientation of the working electrode (WE) and counter electrode (CE) was adjusted so that the WE was placed after the CE in the direction of electrolyte flow. An Ag|AgCl electrode was used as a reference. All electrochemical experiments were conducted in 0.1 M HClO$_4$. Three commercial catalysts (TKK, Japan) consisting of different particle sizes (mean values: 1, 2.6 and 4.8 nm – Fig. 1) dispersed on an HSA support (Vulcan with a Brunauer–Emmett–Teller (BET) surface area of ca. 250 m^2 g^{-1}) are compared in this study. These samples have the characteristics listed in Table 1.

This journal is © the Owner Societies 2017

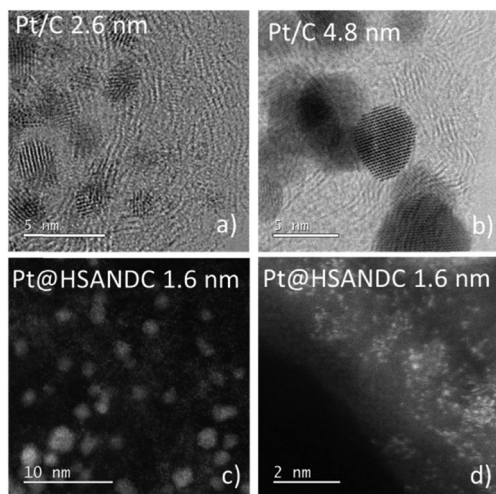*Phys. Chem. Chem. Phys.*, 2017, **19**, 21446–21452 | **21447**

Fig. 1 TEM images of investigated samples. (a) Pt/C sample with an average particle size of 2.6 nm, (b) Pt/C sample with an average particle size of 4.8 nm, and (c and d) Pt@HSANDC with an average particle size of 1.6 nm.

Table 1 Characteristics of the investigated samples with different average particle sizes. Dissolution profiles of Pt/C – 1 nm and Pt/C – 4.8 nm are shown in Fig. S3.1.1 (ESI)

Sample	% Pt	Pt loading [$\mu g\ cm^{-2}_{geo}$]	Carbon loading [$\mu g\ cm^{-2}_{geo}$]
Pt/C – 1 nm	10	7	64
Pt/C – 2.6 nm	46.2	33	38
Pt/C – 4.8 nm	50.8	36	35
Pt@HSANDC	38	28	42

2.2 Electrochemical protocol in EFC-ICP-MS measurements

(A) A fast potentiodynamic experiment was performed: 200 cycles between 0.05 and 1.35 V vs. RHE (300 mV s^{-1}).

(B) A slow potentiodynamic experiment consisting of three consecutive cycles to different upper potential limits (UPLs) at increments of 100 mV (1–1.4 V). For all of the cycles the scan rate was 5 mV s^{-1} whereas the starting potential had a value of 0.05 V vs. RHE.

(C) A potentiostatic experiment with increasing UPLs, with an increment of 200 mV and starting at 0.8 V vs. RHE. Between different UPLs, a potential hold of 0.4 V was employed. Each potential hold lasted for 300 s.

2.3 Synthesis of Pt@HSANDC

The nitrogen-doped porous carbon support used in this study was prepared via an ionothermal method as introduced by Pampel et al.[52] A mixture of adenine (15.00 g, Alfa Aesar), KCl (54.05 g, anhydrous, Sigma Aldrich) and ZnCl$_2$ (98.97 g, anhydrous, Sigma Aldrich) was heated in a quartz furnace under Ar flow in an alumina crucible. The furnace was heated to 900 °C and held at this temperature for 1 h (heating and cooling rates were 2.5 K min^{-1}). The resulting product was washed to remove the salts from the carbon – once in 3 L of 1 M HCl and three times in 3 L of deionized water. Each time the material was dispersed, stirred for several

hours and then filtered. The washed carbon material was finally vacuum-dried overnight at 125 °C. Pt was deposited on the carbon support by mixing 50 mg of carbon with 300 μL of aqueous solution of Pt(NH$_3$)$_4$(NO$_3$)$_2$ (0.39 mM, Alfa Aesar) into a homogeneous paste. The paste was dried at 50 °C in air, and the obtained material was subsequently annealed at 400 °C for 1 h under Ar flow (heating and cooling rates were 5.0 K min^{-1}). The final loading of Pt was 38% (Table 1).

3. Results and discussion

The first aim of the present investigation is to shed light on the effect of heteroatom doped supports with high specific surface areas on the stability of Pt electrocatalysts. Pt nanoparticles with an average particle size of 1.6 nm and a relatively narrow size distribution (Fig. S4.1, ESI†) were formed on high surface area nitrogen-doped carbon supports (HSANDC, BET 2335 m^2 g^{-1}, see Table S1.1, ESI†). Note that in comparison to previously reported N-doped carbon supports e.g. HGS (SSA$_{BET}$ = 1760 m^2 g^{-1}), Pt@HSANDC has a substantially higher specific BET surface area (see Table S1.1, ESI†). This very large BET is presumably one of the reasons that Pt@HSANDC exhibits a significantly different dissolution profile compared to the commercial catalysts (Fig. 2). Generally, the dissolution intensity is lower and the peaks are wider. This indicates that the average transport time of the dissolved Pt ions leaving the catalyst film is longer, that is, the retention time of Pt inside the catalyst is increased. A more detailed analysis however is required to find the deeper underlying reasons for this effect. First it is very important to recognize that the dissolution of Pt is slowed down even if the particle size of Pt in Pt@HSANDC is considerably smaller (ca. 1.6 nm) than in the commercial catalyst (ca. 2.6 nm). Since this is not in line with the particle size effect, one should consider that a non-intrinsic effect dominates the Pt dissolution process in the case of Pt@HSANDC. At least two phenomena need to be considered to explain the non-intrinsic effect: (i) "over-saturation" due to a high local concentration of dissolved Pt ions in the confined pores of HSANDC and (ii) intensive re-deposition of Pt ions which get coordinated with nitrogen surface atoms or
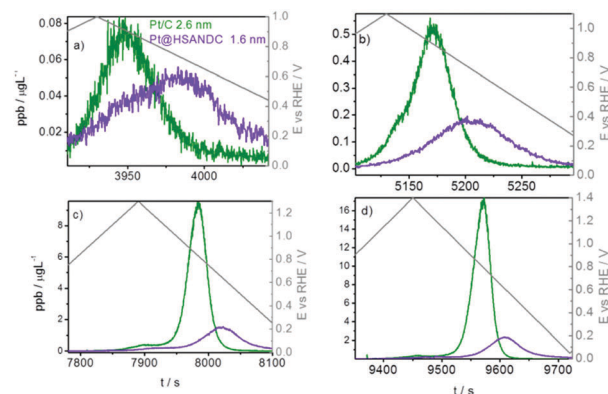

Fig. 2 Time and dissolution vs. potential profile in the slow potentio-dynamic experiment by gradually increasing UPL: (a) 1.0 V, (b) 1.1 V, (c) 1.3 V and (d) 1.4 V.

21448 | Phys. Chem. Chem. Phys., 2017, **19**, 21446–21452

This journal is © the Owner Societies 2017

get electrochemically reduced on Pt particles.[19] In commercial catalysts, these special processes are either absent due to the absence of nanopores (in the case of phenomenon (i)), or significantly less intense due to the absence of N-sites (in the case of phenomenon (ii)). Thus the usual normalization of the dissolution to the real Pt area is not completely justified and is therefore omitted in Fig. 2 (see also discussion in Section S3.1 in the ESI†). Still, we wish to stress that the Pt loading and catalyst film thickness are similar (see Table 1) in both samples (integrated – total amounts of dissolved Pt are listed in Fig. S3.1.3, ESI†). Intuitively, re-deposition is not expected to play a significant role under slow scan rates (5 mV s^{-1}) where sufficient time is given for Pt ions to diffuse to the main flow of the electrolyte before reductive potentials are reached. However, in contrast to this intuition, it has been shown in previous experiments that re-deposition can also have a considerable effect at slow scan rates.[37,43] Thus at this moment we do not wish to exclude any of the possible mechanisms under points (i) and (ii).

To further elucidate the extent of assumed oversaturation and re-deposition phenomena, the following experiment was conducted: additional carbon (Vulcan) was added to suspensions of one of the commercial Pt/C analogues (2.6 nm) to form samples with different Pt:C ratios, that is to dilute Pt in the catalyst film/layer. However, to keep the total Pt content constant, the carbon film thickness on the electrode had to be appropriately adjusted (Table 2).

Rather unexpectedly, in a slow potentiodynamic (5 mV s^{-1}) experiment, the Pt dissolution profiles in samples with different carbon contents show a non-uniform trend (Fig. 3). Upon a moderate increase in the carbon content (red curves in Fig. 3), Pt dissolution is significantly inhibited and the peak position shifted to the right with respect to the original sample having the smallest carbon content (green curve). However, a further increase in the carbon content (blue curves) increases Pt dissolution again and the peaks shift back towards the position of the original/reference sample (green curves). In general, these results clearly demonstrate a pronounced and non-trivial effect of carbon loading on Pt dissolution. In the following, we discuss these results in light of a possible interplay between oversaturation and re-deposition effects.

The trend from the green to the red profile in Fig. 3 is explained as follows. To keep the total Pt content unchanged while adding carbon, the thickness of the catalyst layer had to be appropriately increased. In other words, a given (fixed) Pt amount was "diluted by carbon" by adding more carbon and forming thicker layers (see Scheme S3.2.1, ESI†). Effectively, this means a longer average diffusion path out of a thicker catalyst film. This, in turn, increases the probability for Pt re-deposition before diffusing out of the film. For similar reasons (i.e. due to Pt dilution), the process of oversaturation is more or less excluded,
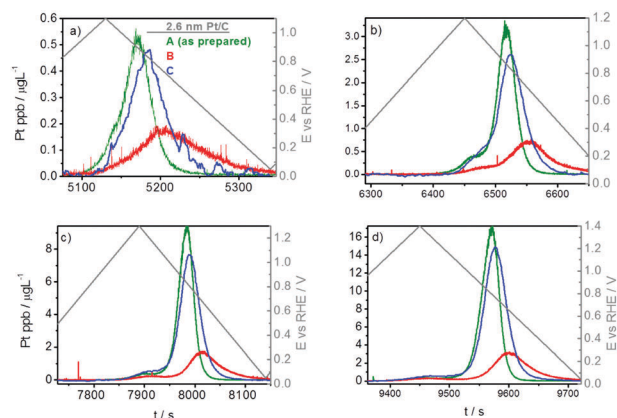

Fig. 3 Time and potentially resolved dissolution profile in the slow potentiodynamic experiment by gradually increasing UPL: (a) 1.1 V, (b) 1.2 V, (c) 1.3 V and (d) 1.4 V.

leaving re-deposition as the governing transport-inhibiting effect in high-surface area Pt/C under slow potentiodynamic regimes.

Based on the above reasoning, one would expect that a further increase in carbon content (film thickness) would result in an even wider and less intensive Pt dissolution profile. However, as mentioned, the opposite trend is observed – the profile resembles the original, non-diluted one (Fig. 3, green curve). It seems as if the effect of re-deposition is not effective anymore in the case of the most diluted Pt. This can be explained as follows: by sufficiently increasing the film thickness, Pt nanoparticles become very much spatially separated; furthermore, it has been shown that Pt re-deposits preferentially on Pt nanoparticles and not on carbon.[19,53] Consequently, in a very diluted system, diffusion of Pt ions out of the catalyst layer is faster in comparison to re-deposition. Therefore, more Pt can "escape" re-deposition and diffuse out of the catalyst layer. This is of significant importance in real catalyst layers as Pt ions diffuse through the membrane until they are reduced by hydrogen that diffuses through the membrane from the anode side. This results in a decreased conductivity of the membrane. According to the results shown in Fig. 3, the ratio between Pt and the carbon support has a strong impact on Pt dissolution. This information is therefore of vital importance for designing real catalyst layers where as low as possible Pt loadings are pursued.

Furthermore, taking into consideration the much higher dispersion of Pt on the porous HSANDC analogue in comparison to the Pt/C analogue, re-deposition should be less likely in the former case. Hence, Pt dissolution should be more intense. Since the opposite trend is noticed (Fig. 2), the inhibited Pt dissolution in the case of the HSANDC analogue should be ascribed to the presence of N atoms which serve as nucleation sites for Pt re-deposition. In terms of real catalyst layers, this means that N doping could be effectively used in stabilizing layers with low Pt loadings.

Taking into account the non-intrinsic dissolution effects of the Pt@HSANDC analogue detected in the slow potentiodynamic experiment discussed above, the dissolution process was

Table 2 Loadings of Pt and carbon on the electrode

Pt/C – 2.6 nm	Pt loading [μg cm$^{-2}_{geo}$]	Carbon loading [μg cm$^{-2}_{geo}$]
A	33	38
B	33	84
C	33	112

This journal is © the Owner Societies 2017

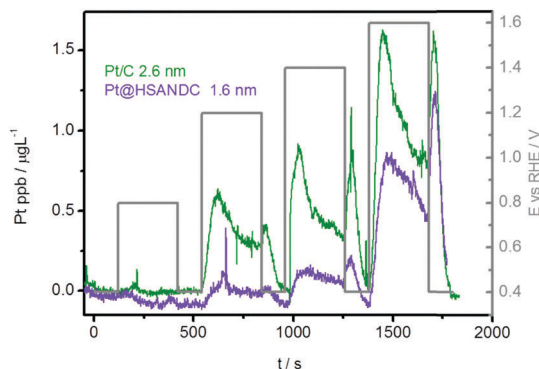*Phys. Chem. Chem. Phys.,* 2017, **19**, 21446–21452 | **21449**

Fig. 4 Time and potential resolved dissolution profile in the potentiostatic experiment. Experimental protocol: the potential was held at 0.8 V and gradually increased by 200 mV up to 1.6 V vs. RHE. Each potential sequence lasted for 5 min. In between each of the sequences, the potential was kept at 0.4 V for 2 min.

Fig. 5 Time and potentially resolved dissolution profile in the fast potentiodynamic experiment; cycling between 0.05 and 1.35 V with a scan rate of 300 mV s^{-1}.

Table 3 ESA retention after 10 000 start/stop RDE degradation cycles of Pt/C and Pt@HSANDC analogues

Sample	ESA retention [%]
Pt@HSANC (1.6 nm)	47
Pt/C (2.6 nm)	29
Pt/C (4.8 nm)	42

further investigated under the potentiostatic regime. A comparison of Pt@HSANDC and the commercial Pt/C analogue is presented in Fig. 4. Pt dissolution is less intense in the case of the Pt@HSANDC sample, which is not in accordance with the particle size effect. Due to the Gibbs–Thomson effect smaller particles should be thermodynamically less stable, hence they should dissolve more readily.[54] A possible explanation would be that smaller particles are more oxophilic, hence more prone to passivation with Pt oxides.[46,47] These inhibit Pt dissolution once a full monolayer is formed. Since the dissolution profiles in Fig. 4 show an unexpected trend, this additionally confirms the confinement effect of Pt ions in the nanopores and also the entrapment effect by coordination/nucleation on N sites of the HSANDC analogue. Here we need to stress that Pt coordinates from the available N ligands result in the formation of single-atom sites.[55–58] These could serve as re-deposition sites at lower potentials.

Based on the above results, we also investigated the dissolution behavior under a fast potentiodynamic regime involving cycling between 0.05 and 1.35 V (Fig. 5). Under fast scan rates, the expected prevailing dissolution mechanism is the direct dissolution of Pt (oxidation of Pt to Pt^{2+}). The so-called "oxide induced" dissolution is minimized due to kinetically hindered formation/reduction of Pt oxide[33,59] and due to the small particle size which is less than 4 nm. Particles below this size were reported to dissolve through a direct dissolution mechanism.[46,47] Dissolution differences between the two analogues should be ascribed to the interplay of particle size effects,[46,47] re-deposition, oversaturation, confinement and entrapment effects. Interestingly, the dissolution profiles of Pt/C and Pt@HSANDC show a completely reverse behavior with respect to the expected particle size effect (Fig. 5). Again, the role of support properties seems to prevail. Specifically, one may expect a more extensive retention of dissolved Pt ions and more effective re-deposition due to the presence of N nucleation sites in the case of the Pt@HSANDC analogue. The potentiodynamic conditions used in Fig. 5 can be related to the real fuel cell conditions when sudden fluctuations of the potential occur pointing to a beneficial employment of the Pt@HSANDC analogue.
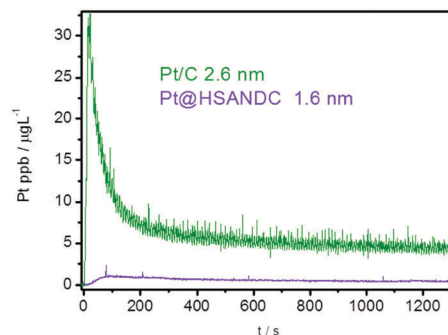
3.1 RDE accelerated start/stop stress tests

Pt@HSANDC (1.6 nm) and Pt/C (both the 2.6 nm and 4.8 nm samples) were subjected to an accelerated start/stop stress test (10.000 cycles between 0.4 and 1.4 V, 1 V s^{-1}) using the rotating disc electrode (RDE) set-up. The primary purpose of these stress tests was to additionally check the main hypothesis of this work – the stabilizing effect of oversaturation and re-deposition on Pt dissolution from different electrode composites. Consistent with the dissolution experiment in Fig. 5, the retention of the electrochemically active surface area (ESA) (Table 3) is substantially larger in the Pt@HSANDC sample compared to the 2.6 nm Pt/C sample, even if the particle size in the former is much smaller (1.6 nm). In comparison to Pt/C with 4.8 nm, the ESA retention is rather similar. This indicates that ESA retention can be further increased if larger particles are dispersed on the HSANDC support.

4. Conclusion

A variety of electrochemical experiments in combination with online analytics have been utilized in order to get a deeper understanding of the complex interplay of various mechanisms occurring during dissolution of Pt catalyst layers from different types of carbon supports. The main conclusions are the following:

(i) Under a slow potentiodynamic regime, the dissolution of Pt nanoparticles from industrial electrocatalysts with different particle sizes follows the well-known particle size effect (i.e., smaller particles dissolve faster).

(ii) When electrocatalysts get diluted, e.g. by the addition of a high-surface area carbon, inconsistencies with respect to established mechanisms are observed. This is because the so-called non-intrinsic effects (that is, effects not dominated by the properties of the metal itself) start to prevail. In particular,

21450 | Phys. Chem. Chem. Phys., 2017, 19, 21446–21452

This journal is © the Owner Societies 2017

oversaturation in nanopores (confinement effect) and re-deposition of Pt presumably on N sites (entrapment effect) have been identified as the dominant non-intrinsic effect.

(iii) Irrespective of the particle size, the dissolution process can be significantly inhibited using a nitrogen-doped, high surface area microporous carbon support. Again, confinement and entrapment are prevailing over the intrinsic effects.

(iv) Overall, nanoparticles dispersed on very high surface area carbon N-doped supports may be seen as a promising direction towards long-term efficiency/stability of the PEMFC catalyst layer (long-term preservation of ESA).

Conflict of interest

There are no conflicts of interest to declare.

Acknowledgements

References

1 I. Katsounaros, S. Cherevko, A. R. Zeradjanin and K. J. J. Mayrhofer, *Angew. Chem., Int. Ed.*, 2014, **53**, 102–121.

2 A. Rabis, P. Rodriguez and T. J. Schmidt, *ACS Catal.*, 2012, **2**, 864–890.

3 P. Jovanovič, A. Pavlišič, V. S. Šelih, M. Šala, N. Hodnik, M. Bele, S. Hočevar and M. Gaberšček, *ChemCatChem*, 2014, **6**, 449–453.

4 S. Cherevko, G. P. Keeley, S. Geiger, A. R. Zeradjanin, N. Hodnik, N. Kulyk and K. J. J. Mayrhofer, *ChemElectroChem*, 2015, **2**, 1471–1478.

5 G. Polymeros, C. Baldizzone, S. Geiger, J. P. Grote, J. Knossalla, S. Mezzavilla, G. P. Keeley, S. Cherevko, a. R. Zeradjanin, F. Schüth and K. J. J. Mayrhofer, *Electrochim. Acta*, 2016, **211**, 744–753.

6 S. Cherevko, N. Kulyk and K. J. J. Mayrhofer, *Nano Energy*, 2016, 1–24.

7 S. Mezzavilla, S. Cherevko, C. Baldizzone, E. Pizzutilo, G. Polymeros and K. J. J. Mayrhofer, *ChemElectroChem*, 2016, **3**, 1524–1536.

8 A. K. Schuppert, a. a. Topalov, I. Katsounaros, S. O. Klemm and K. J. J. Mayrhofer, *J. Electrochem. Soc.*, 2012, **159**, F670–F675.

9 S. Guerin, B. E. Hayden, C. E. Lee, C. Mormiche, J. R. Owen, A. E. Russell, B. Theobald and D. Thompsett, *J. Comb. Chem.*, 2004, **6**, 149–158.

10 J.-P. Grote, A. R. Zeradjanin, S. Cherevko and K. J. J. Mayrhofer, *Rev. Sci. Instrum.*, 2014, **85**, 104101.

11 M. C. Smith, J. A. Gilbert, J. R. Mawdsley, S. Seifert and D. J. Myers, *J. Am. Chem. Soc.*, 2008, **130**, 8112–8113.

12 J. A. Gilbert, A. J. Kropf, N. N. Kariuki, S. DeCrane, X. Wang, S. Rasouli, K. Yu, P. J. Ferreira, D. Morgan and D. J. Myers, *J. Electrochem. Soc.*, 2015, **162**, F1487–F1497.

13 S. O. Klemm, A. A. Topalov, C. A. Laska and K. J. J. Mayrhofer, *Electrochem. Commun.*, 2011, **13**, 1533–1535.

14 K. J. J. Mayrhofer, J. C. Meier, S. J. Ashton, G. K. H. Wiberg, F. Kraus, M. Hanzlik and M. Arenz, *Electrochem. Commun.*, 2008, **10**, 1144–1147.

15 K. Schlögl, K. J. J. Mayrhofer, M. Hanzlik and M. Arenz, *J. Electroanal. Chem.*, 2011, **662**, 355–360.

16 J. C. Meier, I. Katsounaros, C. Galeano, H. J. Bongard, A. A. Topalov, A. Kostka, A. Karschin, F. Schüth and K. J. J. Mayrhofer, *Energy Environ. Sci.*, 2012, **5**, 9319.

17 A. Zana, J. Speder, M. Roefzaad, L. Altmann, M. Baumer and M. Arenz, *J. Electrochem. Soc.*, 2013, **160**, F608–F615.

18 J. C. Meier, C. Galeano, I. Katsounaros, A. A. Topalov, A. Kostka, F. Schüth and K. J. J. Mayrhofer, *ACS Catal.*, 2012, **2**, 832–843.

19 N. Hodnik, M. Zorko, B. Jozinović, M. Bele, G. Dražič, S. Hočevar and M. Gaberšček, *Electrochem. Commun.*, 2013, **30**, 75–78.

20 M. Zorko, B. Jozinović, M. Bele, N. Hodnik and M. Gaberšček, *Ultramicroscopy*, 2014, **140**, 44–50.

21 N. Hodnik, M. Zorko, M. Bele, S. Hočevar, M. Gaberšček, S. Hoc and M. Gabers, *J. Phys. Chem. C*, 2012, **116**, 21326–21333.

22 N. Hodnik, G. Dehm and K. J. J. Mayrhofer, *Acc. Chem. Res.*, 2016, **49**, 2015–2022.

23 J. C. Meier, C. Galeano, I. Katsounaros, J. Witte, H. J. Bongard, A. A. Topalov, C. Baldizzone, S. Mezzavilla, F. Schüth and K. J. J. Mayrhofer, *Beilstein J. Nanotechnol.*, 2014, **5**, 44–67.

24 E. Antolini, J. R. C. Salgado and E. R. Gonzalez, *J. Power Sources*, 2006, **160**, 957–968.

25 J. Zhang, K. Sasaki, E. Sutter and R. R. Adzic, *Science*, 2007, **315**, 220–222.

26 K. Sasaki, H. Naohara, Y. Choi, Y. Cai, W.-F. Chen, P. Liu and R. R. Adzic, *Nat. Commun.*, 2012, **3**, 1115.

27 Y. Kang, J. Snyder, M. Chi, D. Li, K. L. More, N. M. Markovic and V. R. Stamenkovic, *Nano Lett.*, 2014, **14**, 6361–6367.

28 C. Wang, D. Van Der Vliet, K. L. More, N. J. Zaluzec, S. Peng, S. Sun, H. Daimon, G. Wang, J. Pearson, A. P. Paulikas, G. Karapetrov, D. Strmcnik, N. M. Markovic and V. R. Stamenkovic, *Nano Lett.*, 2011, **11**, 919–926.

29 M. Gatalo, P. Jovanovič, G. Polymeros, J.-P. Grote, A. Pavlišič, F. Ruiz- Zepeda, V. S. Šelih, M. Šala, S. Hočevar, M. Bele, K. J. J. Mayrhofer, N. Hodnik and M. Gaberšček, *ACS Catal.*, 2016, **6**, 1630–1634.

30 C. Baldizzone, S. Mezzavilla, H. W. P. Carvalho, J. C. Meier, A. K. Schuppert, M. Heggen, C. Galeano, J.-D. Grunwaldt, F. Schüth and K. J. J. Mayrhofer, *Angew. Chem., Int. Ed.*, 2014, **53**, 14250–14254.

31 C. Galeano, J. C. Meier, M. Soorholtz, H. Bongard, C. Baldizzone, K. J. J. Mayrhofer and F. Schüth, *ACS Catal.*, 2014, **4**, 3856–3868.

32 X. Tuaev, S. Rudi and P. Strasser, *Catal. Sci. Technol.*, 2016, **6**, 8276–8288.

33 A. A. Topalov, S. Cherevko, A. R. Zeradjanin, J. C. Meier, I. Katsounaros and K. J. J. Mayrhofer, *Chem. Sci.*, 2014, **5**, 631–638.

This journal is © the Owner Societies 2017

Phys. Chem. Chem. Phys., 2017, **19**, 21446–21452 | **21451**

34 A. A. Topalov, I. Katsounaros, M. Auinger, S. Cherevko, J. C. Meier, S. O. Klemm and K. J. J. Mayrhofer, *Angew. Chem., Int. Ed.*, 2012, **51**, 12613–12615.

35 S. Cherevko, A. R. Zeradjanin, G. P. Keeley and K. J. J. Mayrhofer, *J. Electrochem. Soc.*, 2014, **161**, H822–H830.

36 M. Łukaszewski and A. Czerwiński, *J. Electroanal. Chem.*, 2006, **589**, 38–45.

37 P. Jovanovič, V. S. Šelih, M. Šala, S. Hočevar, F. Ruiz-Zepeda, N. Hodnik, M. Bele and M. Gaberšček, *Electrochim. Acta*, 2016, **211**, 851–859.

38 C. Baldizzone, L. Gan, N. Hodnik, G. P. Keeley, A. Kostka, M. Heggen, P. Strasser and K. J. J. Mayrhofer, *ACS Catal.*, 2015, **5**, 5000–5007.

39 G. P. Keeley, S. Cherevko and K. J. J. Mayrhofer, *ChemElectroChem*, 2016, **3**, 51–54.

40 T. Nagai, H. Murata and Y. Morimoto, *J. Electrochem. Soc.*, 2014, **161**, F789–F794.

41 K. Yu, D. J. Groom, X. Wang, Z. Yang, M. Gummalla, S. C. Ball, D. J. Myers and P. J. Ferreira, *Chem. Mater.*, 2014, **26**, 5540–5548.

42 H. Yano, M. Watanabe, A. Iiyama and H. Uchida, *Nano Energy*, 2016, 1–11.

43 A. A. Topalov, A. R. Zeradjanin, S. Cherevko and K. J. J. Mayrhofer, *Electrochem. Commun.*, 2014, **40**, 49–53.

44 P. Bindra, *J. Electrochem. Soc.*, 1979, **126**, 1631.

45 P. Jovanovič, V. S. Šelih, M. Šala, S. B. Hočevar, A. Pavlišič, M. Gatalo, M. Bele, F. Ruiz-Zepeda, M. Čekada, N. Hodnik and M. Gaberšček, *J. Power Sources*, 2016, **327**, 675–680.

46 L. Tang, B. Han, K. Persson, C. Friesen, T. He, K. Sieradzki and G. Ceder, *J. Am. Chem. Soc.*, 2010, **132**, 596–600.

47 L. Tang, X. Li, R. C. Cammarata, C. Friesen and K. Sieradzki, *J. Am. Chem. Soc.*, 2010, **132**, 11722–11726.

48 E. F. Holby, W. Sheng, Y. Shao-Horn and D. Morgan, *Energy Environ. Sci.*, 2009, **2**, 865.

49 Y. Shao-Horn, W. C. Sheng, S. Chen, P. J. Ferreira, E. F. Holby and D. Morgan, *Top. Catal.*, 2007, **46**, 285–305.

50 Y. Zhou, K. Neyerlin, T. S. Olson, S. Pylypenko, J. Bult, H. N. Dinh, T. Gennett, Z. Shao and R. O'Hayre, *Energy Environ. Sci.*, 2010, **3**, 1437.

51 X. Li, S. Park and B. N. Popov, *J. Power Sources*, 2010, **195**, 445–452.

52 J. Pampel and T.-P. Fellinger, *Adv. Energy Mater.*, 2016, **6**, 1502389.

53 N. Hodnik, B. Jozinović, M. Zorko and M. Gaberšček, *Acta Chim. Slov.*, 2014, **61**, 280–283.

54 W. Sheng, S. Chen, E. Vescovo and Y. Shao-Horn, *J. Electrochem. Soc.*, 2012, **159**, B96.

55 D. A. Bulushev, M. Zacharska, A. S. Lisitsyn, O. Y. Podyacheva, F. S. Hage, Q. M. Ramasse, U. Bangert and L. G. Bulusheva, *ACS Catal.*, 2016, **6**, 3442–3451.

56 L. Jia, D. A. Bulushev, O. Y. Podyacheva, A. I. Boronin, L. S. Kibis, E. Y. Gerasimov, S. Beloshapkin, I. A. Seryak, Z. R. Ismagilov and J. R. H. Ross, *J. Catal.*, 2013, **307**, 94–102.

57 Y.-H. Li, T.-H. Hung and C.-W. Chen, *Carbon*, 2009, **47**, 850–855.

58 M. N. Groves, A. S. W. Chan, C. Malardier-Jugroot and M. Jugroot, *Chem. Phys. Lett.*, 2009, **481**, 214–219.

59 N. Hodnik, C. Baldizzone, S. Cherevko, A. Zeradjanin and K. J. J. Mayrhofer, *Electrocatalysis*, 2015, **6**, 237–241.

21452 | *Phys. Chem. Chem. Phys.*, 2017, **19**, 21446–21452

This journal is © the Owner Societies 2017